Applied Catalysis B: Environmental 110 (2011) 71–80

Contents lists available at SciVerse ScienceDirect

Applied Catalysis B: Environmental

journal homepage: www.elsevier.com/locate/apcatb

Low temperature selective catalytic reduction of NO with NH_3 over Mn–Fe spinel: Performance, mechanism and kinetic study

Shijian Yang[a,b], Chizhong Wang[a], Junhua Li[a,*], Naiqiang Yan[b,*], Lei Ma[a], Huazheng Chang[a]

[a] School of Environment, Tsinghua University, Beijing, 100084, PR China
[b] School of Environmental Science and Engineering, Shanghai Jiao Tong University, Shanghai, 200240, PR China

ARTICLE INFO

Article history:
Received 27 May 2011
Received in revised form 30 July 2011
Accepted 19 August 2011
Available online 25 August 2011

Keywords:
Low temperature SCR
$(Fe_{3-x}Mn_x)_{1-\delta}O_4$
Kinetic analysis
N_2O origination

ABSTRACT

$(Fe_{3-x}Mn_x)_{1-\delta}O_4$ was synthesized using a co-precipitation method and then developed as a catalyst for the low temperature selective catalytic reduction (SCR) of NO with NH_3. The SCR activity of $(Fe_{3-x}Mn_x)_{1-\delta}O_4$ was clearly enhanced with the increase of Mn content. The results of in situ DRIFTS study demonstrated that both the Eley–Rideal mechanism (i.e. reaction of activated ammonia with gaseous NO) and the Langmuir–Hinshelwood mechanism (i.e. reaction of adsorbed ammonia species with adsorbed NO_x species) might happen during the SCR reaction over $(Fe_{3-x}Mn_x)_{1-\delta}O_4$. According to the kinetic analysis, the respective contribution of the Langmuir–Hinshelwood mechanism and the Eley–Rideal mechanism on the SCR reaction was studied. Only the adsorption of NO + O_2 on $(Fe_{2.8}Mn_{0.2})_{1-\delta}O_4$ was promoted, so the Langmuir–Hinshelwood mechanism predominated over NO conversion on $(Fe_{2.8}Mn_{0.2})_{1-\delta}O_4$ especially at lower temperatures. Both the adsorption of NO + O_2 and the adsorption of NH_3 on $(Fe_{2.5}Mn_{0.5})_{1-\delta}O_4$ were obviously promoted, so NO conversion on $(Fe_{2.5}Mn_{0.5})_{1-\delta}O_4$ mainly followed the Eley–Rideal mechanism especially at higher temperatures. Both the nitrate route and the over-oxidization of adsorbed ammonia species contributed to the formation of N_2O on $(Fe_{2.8}Mn_{0.2})_{1-\delta}O_4$ above 140 °C. However, the formation of N_2O on $(Fe_{2.5}Mn_{0.5})_{1-\delta}O_4$ mainly resulted from the over-oxidization of adsorbed ammonia species. Although the activity of $(Fe_{2.5}Mn_{0.5})_{1-\delta}O_4$ was suppressed in the presence of H_2O and SO_2, the deactivated catalyst can be regenerated after the water washing.

1. Introduction

Nitrogen oxides (NO and NO_2), which result from automobile exhaust gas and industrial combustion of fossil fuels, have been a major pollutant for air pollution [1–4]. They contribute to photochemical smog, acid rain, ozone depletion and greenhouse effect [1,5–7]. Selective catalytic reduction (SCR) of NO with NH_3 has been an efficient technique for the control of NO_x emission from coal fired power plants and automobiles. V_2O_5–WO_3(MoO_3)/TiO_2 has been widely used as a SCR catalyst to control the emission of NO_x from stationary coal fired power plants and automobiles for several decades [3,8–10]. The SCR unit is located upstream of the desulfurizer and electrostatic precipitator in order to avoid reheating of the flue gas. The problems of this system are as follows: the relatively narrow temperature window (350–400 °C), the low N_2 selectivity in the high temperature range, the toxicity of vanadium pentoxide to the environment, the high conversion of SO_2 to SO_3, and the deposition of dust on the catalyst [3,4,8–13].

For the above reasons, there has been strong interest in developing highly active catalysts for low temperature SCR, which would be placed downstream electrostatic precipitator and desulfurizer [14–17]. Previous researches have demonstrated that some Mn based catalysts showed an excellent activity for the low temperature SCR reaction [10,18–29]. So far, there is no agreement on the way the low temperature SCR reaction continues: by (1) reaction of gaseous NO with (activated) NH_3 to an activated transition state and subsequent decomposition to N_2 and H_2O (i.e. the Eley–Rideal mechanism), or (2) adsorption of NO on the adjacent sites of adsorbed NH_3, followed by reaction to an activated transition state and decomposition to the reaction products (the Langmuir–Hinshelwood mechanism) [21,25].

Over the past few years, Mn–Fe spinel $(Fe_{3-x}Mn_x)_{1-\delta}O_4$ nanoparticles have attracted considerable attention due to their reportedly improved performance as catalysts in Fischer–Tropsh synthesis [30]. Our previous research has demonstrated that $(Fe_{3-x}Mn_x)_{1-\delta}O_4$ was an excellent magnetic catalyst/sorbent for the oxidization and capture of elemental mercury from the flue gas [31].

Herein, nanosized $(Fe_{3-x}Mn_x)_{1-\delta}O_4$ was developed as a super catalyst for the low temperature SCR of NO_x with NH_3. $(Fe_{3-x}Mn_x)_{1-\delta}O_4$ was synthesized using a co-precipitation

* Corresponding author. Tel.: +86 10 62771093; fax: +86 10 62771093.
E-mail addresses: lijunhua@tsinghua.edu.cn (J. Li), nqyan@sjtu.edu.cn (N. Yan).

0926-3373/$ – see front matter © 2011 Elsevier B.V. All rights reserved.
doi:10.1016/j.apcatb.2011.08.027

method and then characterized using X-ray diffraction (XRD), NH_3 temperature programmed desorption (NH_3-TPD), N_2 adsorption/desorption isotherm and X-ray photoelectron spectroscopy (XPS). Subsequently, a fixed-bed reactor system was used to investigate the low temperature SCR performance of $(Fe_{3-x}Mn_x)_{1-\delta}O_4$. Furthermore, the mechanism of the low temperature SCR reaction over $(Fe_{3-x}Mn_x)_{1-\delta}O_4$ was investigated using in situ DRIFTS study and kinetic analysis.

2. Experimental

2.1. Catalyst preparation

Nanosized $Fe_{3-x}Mn_xO_4$, the precursor of $(Fe_{3-x}Mn_x)_{1-\delta}O_4$ was prepared using a co-precipitation method [31–33]. Suitable amounts of ferrous sulfate, ferric chloride, and manganese sulfate were dissolved in distilled water (total cation concentration = 0.30 mol L^{-1}). Then, the mixture was added to an ammonia solution, leading to an instantaneous precipitation of manganese ferrite. During the reaction, the system was continuously stirred at 800 rpm. The particles were then separated by centrifugation at 4500 rpm for 5 min and washed with distilled water followed by a new centrifugation. After 3 washings, the particles were collected and dried in a vacuum oven at 105 °C for 12 h. γ-Fe_2O_3 was obtained after the thermal treatment of Fe_3O_4 under air at 250 °C for 3 h. $(Fe_{3-x}Mn_x)_{1-\delta}O_4$ (x = 0.2 and 0.5) were obtained after the thermal treatment of $Fe_{3-x}Mn_xO_4$ under air at 400 °C for 3 h.

2.2. Catalyst characterization

Powder XRD pattern was recorded on an X-ray diffractionmeter (Rigaku, D/max-2200/PC) between 10° and 80° at a step of 7° min^{-1} operating at 30 kV and 30 mA using Cu Kα radiation. BET surface area was determined using a nitrogen adsorption apparatus (Micromeritics, ASAP 2010 M + C). The sample was outgassed at 200 °C before BET measurement. The acidity on $(Fe_{3-x}Mn_x)_{1-\delta}O_4$ was determined using NH_3-TPD. NH_3-TPD was carried out on a chemisorption analyzer (Micromeritics, AutoChem 2920). Before the experiment, about 0.15 g of catalyst was pretreated under He atmosphere at 300 °C for 60 min to remove the adsorbed H_2O and other gases. After the catalyst was cooled to 50 °C, the He flow was switched to a flow of 10% NH_3/He (15 mL min^{-1}) for 60 min. The sample was then purged by He (30 mL min^{-1}) for another 60 min. NH_3-TPD was preformed at a heating rate of 10 °C min^{-1} to 500 °C under He atmosphere. XPS (Thermo, ESCALAB 250) with Al Kα ($h\nu$ = 1486.6 eV) as the excitation source was used to determine the binding energies of Fe 2p, Mn 2p and O1s. The C1s line at 284.6 eV was taken as a reference for the binding energy calibration.

2.3. Catalytic test

The SCR tests were performed on a fixed-bed quartz tube reactor (6 mm internal diameter) containing 100 mg of catalyst (40–60 mesh). The typical reactant gas composition was as follows: 500 ppm of NO, 500 ppm of NH_3, 2 vol% of O_2, and balance of N_2. The total flow rate ranged from100 to 400 mL min^{-1}, and the gas hourly space velocity (GHSV) varied from 3.75×10^4 to 3.0×10^5 h^{-1}. The concentrations of NO and NO_2 were continually monitored by a chemiluminescent NO/NO_x analyzer (Thermo, Model 42*i*-HL). Meanwhile, the concentrations of NH_3 and N_2O were continually monitored by a FTIR spectrometer (Gasmet FTIR DX4000).

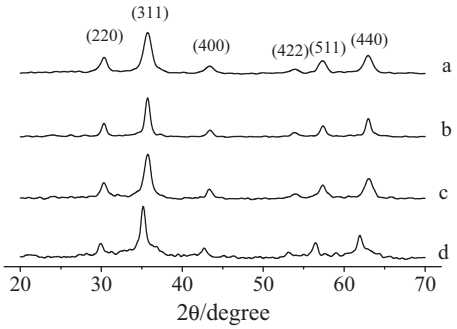

Fig. 1. XRD patterns of synthesized $(Fe_{3-x}Mn_x)_{1-\delta}O_4$: (a) x = 0; (b) x = 0.2; (c) x = 0.5; (d) x = 0.5 before the calcination.

The pseudo-first order rate constant (k) of the SCR reaction was calculated according to Eq. (1).

$$k = -\frac{F_0}{[NO]_0 W} \ln(1 - X) \quad (1)$$

where F_0 was the molar NO feed rate, $[NO]_0$ was the molar NO concentration at the inlet (at reaction temperature), W was the mass of catalyst (g) and X was the ratio of NO conversion.

2.4. In situ DRIFTS study

In situ DRIFT spectra were recorded on a Fourier transform infrared spectrometer (FTIR, Nicolet NEXUS 870) equipped with a smart collector and an MCT detector cooled by liquid N_2. The diffuse reflectance measurements were carried out in situ in a high temperature cell with ZnSe windows. The fine catalyst was placed in a ceramic crucible and manually pressed. Mass flow controllers and a sample temperature controller were used to simulate the real reactions. Prior to each experiment, the catalyst was heated at 300 °C in a flow of N_2 (100 mL min^{-1}) for 120 min. The FTIR spectra were recorded by accumulating 100 scans with a resolution of 4 cm^{-1}.

3. Results and discussion

3.1. Characterization

3.1.1. XRD

The characteristic reflections of synthesized catalysts (shown in Fig. 1) correspond very well to the standard card of maghemite (JCPDS: 39-1346). Additional reflections that would indicate the presence of other crystalline manganese oxides, such as Mn_3O_4, Mn_2O_3 or MnO_2, were not present in the diffraction scan. Because the radiuses of Mn^{2+} (0.80 Å) and Mn^{3+} (0.66 Å) are bigger than those of Fe^{2+} (0.74 Å) and Fe^{3+} (0.64 Å) respectively, the lattice parameter of synthesized $Fe_{2.5}Mn_{0.5}O_4$ (0.8446 nm) was much larger than that of magnetite (0.8396 nm) [34]. These results indicate that Mn cations were incorporated into the spinel structure. Because the radiuses of Fe^{2+} and Mn^{2+} are larger than those of Fe^{3+}, Mn^{3+} and Mn^{4+} (0.60 Å), the lattice parameter of $Fe_{2.5}Mn_{0.5}O_4$ decreased after the oxidization of Fe^{2+} and Mn^{2+} cations (shown in Table 1) [31].

Table 1
Lattice parameter, BET surface area, acidity of $(Fe_{3-x}Mn_x)_{1-\delta}O_4$.

	Lattice parameter/nm	BET surface area/m^2 g^{-1}	Acidity/μmol m^{-2}
x = 0	0.8326	88.5	6.6
x = 0.2	0.8324	68.0	6.8
x = 0.5	0.8332	101	7.5

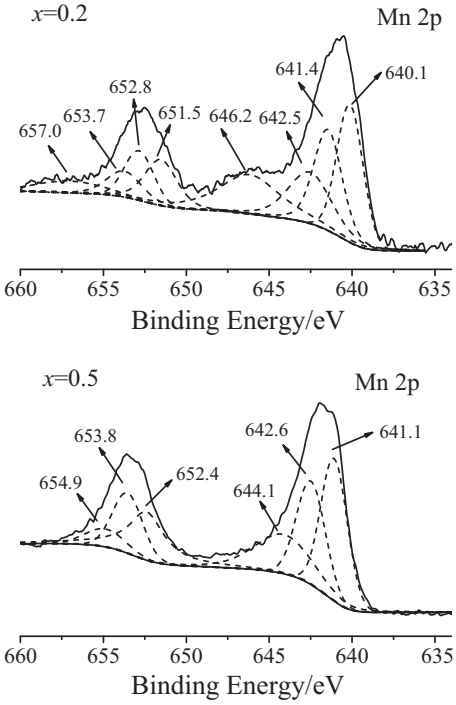

Fig. 2. XPS spectra of $(Fe_{3-x}Mn_x)_{1-\delta}O_4$ over the spectral region of Mn 2p.

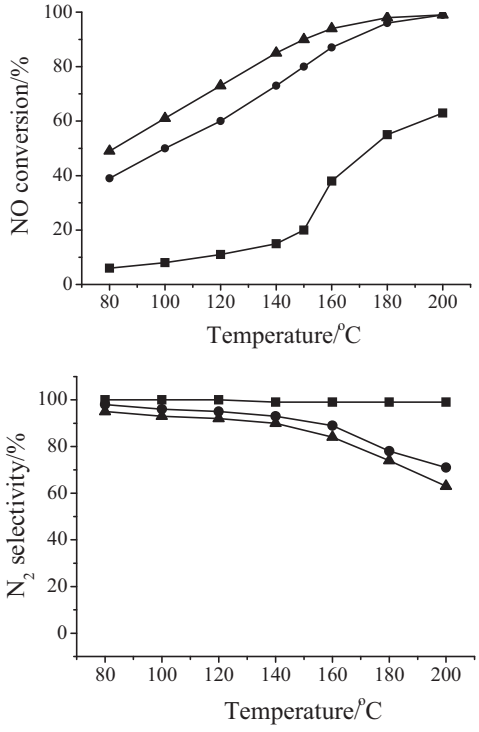

Fig. 3. SCR performance of $(Fe_{3-x}Mn_x)_{1-\delta}O_4$: ■, $x=0$; •, $x=0.2$; ▲, $x=0.5$. (a) NO conversion; (b) N_2 selectivity. Reaction condition: [NO] = [NH_3] = 500 ppm, [O_2] = 2 vol%, N_2 balance, catalyst mass = 100 mg, total flow rate = 200 mL min^{-1} and GHSV = 150,000 h^{-1}.

Table 2
Percents of Fe^{3+}, Mn^{2+}, Mn^{3+} and Mn^{4+} on $(Fe_{3-x}Mn_x)_{1-\delta}O_4$/%.

	Fe^{3+}	Mn^{2+}	Mn^{3+}	Mn^{4+}
$x=0$	40	–	–	–
$x=0.2$	35.3	1.9	1.6	1.6
$x=0.5$	26.7	–	7.6	6.0

3.1.2. XPS

Surface information on synthesized catalyst was analyzed by XPS. XPS spectra over the spectral regions of Fe 2p, Mn 2p and O1s were evaluated.

Fe species on $(Fe_{3-x}Mn_x)_{1-\delta}O_4$ were assigned to oxidized Fe species (figure was not shown), more likely Fe^{3+} type species [31,35]. The binding energies centered at about 709.8 and 711.0 eV may be assigned to Fe^{3+} cations in the spinel structure, and the binding energy centered at about 712.3 eV may be ascribed to Fe^{III}–OH [36]. The binding energy of O1s mainly centered at about 529.8 eV, as expected for the transition metal oxides (figure was not shown). Another oxygen species at about 531.4 eV was also observed, which was assigned to –OH [37].

Fig. 2 shows the XPS spectra over the spectral region of Mn 2p. As 6.7% of Fe^{3+} cations were substituted by Mn cations, Mn^{2+} (640.1 eV), Mn^{3+} (641.4 eV) and Mn^{4+} (642.5 eV) appeared on $(Fe_{2.8}Mn_{0.2})_{1-\delta}O_4$ [31]. With the further increase of Mn content, the Mn species on $(Fe_{2.5}Mn_{0.5})_{1-\delta}O_4$ were mainly assigned to Mn^{4+} (642.6 eV) and Mn^{3+} (641.1 eV). As shown in Table 2, the percent of Mn^{4+} cation on $(Fe_{3-x}Mn_x)_{1-\delta}O_4$ obviously increased with the increase of Mn content.

3.2. Catalytic performance

Fig. 3 shows the low temperature SCR performance of $(Fe_{3-x}Mn_x)_{1-\delta}O_4$. The ratio of NO conversion increased with the increase of Mn content in the spinel (shown in Fig. 3a). It indicates that the SCR activity of $(Fe_{3-x}Mn_x)_{1-\delta}O_4$ was obviously promoted due to the incorporation of Mn into the spinel structure. Meanwhile, NO conversion increased with the increase of reaction temperature. $(Fe_{3-x}Mn_x)_{1-\delta}O_4$ showed an excellent N_2 selectivity below 140 °C (>90%). However, N_2 selectivity obviously decreased with the further increase of reaction temperature. Meanwhile, the amount of N_2O formed increased with the increase of Mn content (shown in Fig. 3b).

A summary comparison has been made for $(Fe_{2.5}Mn_{0.5})_{1-\delta}O_4$ with other high-activity Mn based catalysts that were reported in the literature. In order for a fair comparison, the pseudo-first rate constants, k, were calculated by Eq. (1), assuming diffusion-limitation free. As shown in Table 3, k of $(Fe_{2.5}Mn_{0.5})_{1-\delta}O_4$ at 150 °C

Table 3
Performance of various catalysts for low temperature SCR of NO with NH_3.

Catalyst	Feed composition			t (°C)	X (%)	GHSV (h^{-1})	k ($cm^3\ g^{-1}\ s^{-1}$)
	NO (ppm)	NH_3 (ppm)	O_2 (%)				
$(Fe_{2.5}Mn_{0.5})_{1-\delta}O_4$	500	500	2	150	90	150,000	109
MnO_x/Al_2O_3 [38]	500	550	2	150	63	24,000	9.4
MnO_x–WO_3/γ-Al_2O_3 [39]	500	550	10	150	45	91,400	21.5
MnO_x–CeO_2 [23]	1000	1000	2	150	87	210,000	121
Fe–Mn/TiO_2 [22]	1000	1000	2	150	75	150,000	65.6
Mn/TiO_2 [22]	1000	1000	2	150	90	30,000	21.8
Mn/TiO_2 [28]	400	400	2	175	85	50,000	44.9

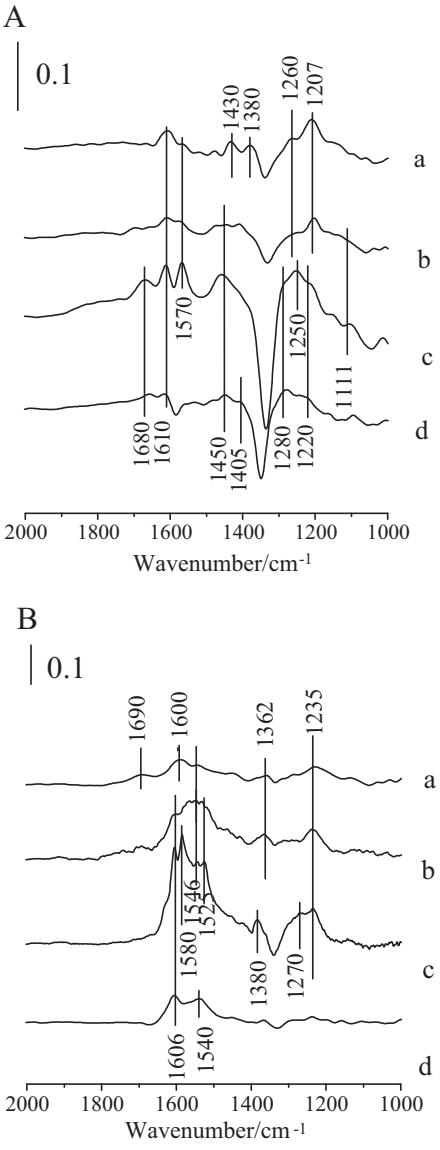

Fig. 4. (A) DRIFT spectra of the adsorption of NH_3 on $(Fe_{3-x}Mn_x)_{1-\delta}O_4$; (B) DRIFT spectra of the adsorption of $NO_2 + O_2$ on $(Fe_{3-x}Mn_x)_{1-\delta}O_4$. (a) $x = 0$ at 120 °C; (b) $x = 0.2$ at 120 °C; (c) $x = 0.5$ at 120 °C; (d) $x = 0.5$ at 180 °C.

was close to that of MnO_x–CeO_2 [23], and it was much more than those of MnO_x/Al_2O_3 [38], Mn_2O_3–WO_3/γ-Al_2O_3 [39], Mn/TiO_2 [22,28] and Fe–Mn/TiO_2 [22].

3.3. DRIFTS Study

3.3.1. Adsorption of NH_3 and $NO + O_2$ on $(Fe_{3-x}Mn_x)_{1-\delta}O_4$

After the adsorption of NH_3 on γ-Fe_2O_3 at 120 °C, five bands at 1610, 1430, 1380, 1260 and 1207 cm^{-1} appeared (shown in Fig. 4A-a). The bands at 1610 and 1207 cm^{-1} were assigned to coordinated NH_3 bound to the Lewis acid sites, and the band at 1430 cm^{-1} was attributed to ionic NH_4^+ bound to the Brønsted acid sites [9,25]. The bands at 1380 and 1260 cm^{-1} may be attributed to the oxidization/deformation species of adsorbed ammonia species [25]. As 6.7% of Fe^{3+} cations in γ-Fe_2O_3 were substituted by Mn cations, no obvious changes happened in the FTIR spectra of $(Fe_{2.8}Mn_{0.2})_{1-\delta}O_4$ after the adsorption of NH_3 at 120 °C (shown in Fig. 4A-b). With the further increase of Mn content, the bands corresponding to adsorbed ammonia species on $(Fe_{2.5}Mn_{0.5})_{1-\delta}O_4$ obviously increased (shown in Fig. 4A-c). This result was consistent with the result of NH_3-TPD (shown in Table 1). As the adsorption temperature increased from 120 to 180 °C, the adsorption of ammonia species on $(Fe_{2.5}Mn_{0.5})_{1-\delta}O_4$ obviously decreased. It indicates that the adsorption of NH_3 on $(Fe_{2.5}Mn_{0.5})_{1-\delta}O_4$ was restrained with the increase of reaction temperature.

After the adsorption of $NO + O_2$ on γ-Fe_2O_3 at 120 °C, five bands at 1690, 1600, 1546, 1362 and 1235 cm^{-1} appeared (shown in Fig. 4B-a). The band at 1690 cm^{-1} may be attributed to adsorbed NO, and the bands at 1600, 1546, 1362 and 1235 cm^{-1} were assigned to monodentate nitrite [40]. As Mn was incorporated into the spinel structure, two new bands at 1580 and 1525 cm^{-1} appeared and the band at 1690 cm^{-1} disappeared. The bands at 1580 and 1525 cm^{-1} were assigned to bidentate nitrate [40]. Previous researches suggested that bidentate nitrate resulted from the further oxidization of monodentate nitrite [21,40]. With the increase of Mn content, the adsorption of $NO + O_2$ obviously increased (shown in Fig. 4B). It indicates that the adsorption of $NO + O_2$ on γ-Fe_2O_3 was obviously promoted due to the incorporation of Mn. As the adsorption temperature increased from 120 to 180 °C, the adsorption of $NO + O_2$ on $(Fe_{2.5}Mn_{0.5})_{1-\delta}O_4$ obviously decreased (shown in Fig. 4B-d). The bands at 1580 and 1525 cm^{-1} corresponding to bidentate nitrate disappeared, and a new band at 1540 cm^{-1} corresponding to monodentate nitrate appeared.

3.3.2. Reaction between nitrogen oxide and ammonia

$(Fe_{2.5}Mn_{0.5})_{1-\delta}O_4$ was first treated with NH_3/N_2 for 1 h followed by N_2 purged for 30 min at 120 °C. $NO + O_2/N_2$ was then introduced into the IR cell (shown in Fig. 5a). After the adsorption of NH_3, $(Fe_{2.5}Mn_{0.5})_{1-\delta}O_4$ were mainly covered by coordinated NH_3 (at 1609 and 1210 cm^{-1}) bound to the Lewis acid sites, ionic NH_4^+ (at 1680 and 1450 cm^{-1}) bound to the Brønsted acid sites and the oxidization/deformation species of adsorbed ammonia (at 1570 and 1260 cm^{-1}) [9]. After $NO + O_2/N_2$ passed over NH_3 pretreated $(Fe_{2.5}Mn_{0.5})_{1-\delta}O_4$, the bands at 1680, 1210 and 1450 cm^{-1} corresponding to adsorbed ammonia species diminished. Meanwhile, monodentate nitrite (1607, 1550 cm^{-1}) and bidentate nitrate (1580 and 1525 cm^{-1}) appeared. As the reaction temperature increased from 120 to 180 °C, monodentate nitrite (1606 cm^{-1}) and monodentate nitrate (1540 cm^{-1}) appeared after $NO + O_2$ passed through the NH_3 pretreated $(Fe_{2.5}Mn_{0.5})_{1-\delta}O_4$ (shown in Fig. 5b). These results suggest both the coordinated NH_3 and ionic NH_4^+ can take part in the SCR reaction.

Then, the reactants were introduced to $(Fe_{2.5}Mn_{0.5})_{1-\delta}O_4$ in the reversed order. $(Fe_{2.5}Mn_{0.5})_{1-\delta}O_4$ was first treated with $NO + O_2/N_2$ for 1 h followed by N_2 purged for 30 min at 120 °C. NH_3/N_2 was then introduced into the IR cell (shown in Fig. 5c). After the adsorption of $NO + O_2$ at 120 °C, $(Fe_{2.5}Mn_{0.5})_{1-\delta}O_4$ was mainly covered by monodentate nitrite (1606, 1546 and 1235 cm^{-1}) and bidentate nitrate (1580 and 1525 cm^{-1}). After NH_3 was introduced into the cell, the bands corresponding to monodentate nitrite (1606, 1546 and 1235 cm^{-1}) disappeared. Meanwhile, the bands at 1680, 1609 and 1444 cm^{-1} corresponding to the adsorbed ammonia species appeared. However, the bands at about 1570 and 1505 cm^{-1} corresponding to bidentate nitrate were still present. Because the bidentate nitrate was bound with adsorbed ammonia species, they shifted to low wavenumber. It indicates that only monodentate nitrite took part in the SCR reaction and bidentate nitrate cannot react with ammonia to form H_2O and N_2 at 120 °C. As the reaction temperature increased from 120 to 180 °C, $(Fe_{2.5}Mn_{0.5})_{1-\delta}O_4$ were mainly covered by monodentate nitrate (1540 cm^{-1}) and monodentate nitrite (1606 cm^{-1}) after the adsorption of $NO + O_2$. Because monodentate nitrate and monodentate nitrite were bound with adsorbed ammonia species after the introduction of NH_3, they first shifted to 1560 and 1510 cm^{-1}. Then, both the adsorbed nitrate and nitrite gradually decreased (shown in Fig. 5d). It indicates that both adsorbed nitrate and nitrite can take part in the SCR reaction at

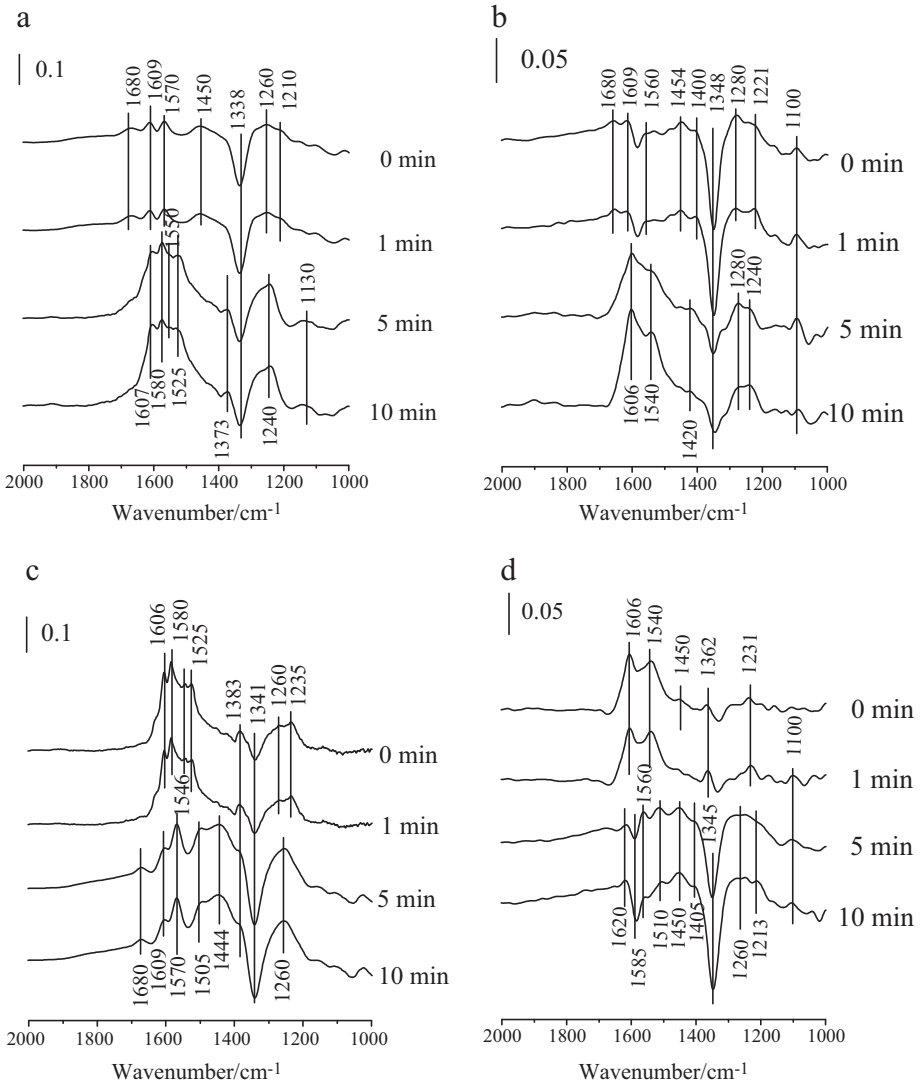

Fig. 5. (a) DRIFT spectra taken at 120 °C upon passing NO + O_2 over the NH_3 presorbed $(Fe_{2.5}Mn_{0.5})_{1-\delta}O_4$; (b) DRIFT spectra taken at 180 °C upon passing NO + O_2 over the NH_3 presorbed $(Fe_{2.5}Mn_{0.5})_{1-\delta}O_4$; (c) DRIFT spectra taken at 120 °C upon passing NH_3 over the NO + O_2 presorbed $(Fe_{2.5}Mn_{0.5})_{1-\delta}O_4$; (d) DRIFT spectra taken at 180 °C upon passing NH_3 over the NO + O_2 presorbed $(Fe_{2.5}Mn_{0.5})_{1-\delta}O_4$.

180 °C. Fig. 5d also shows that the decrease of monodentate nitrite was much faster than that of monodentate nitrate. It suggests that the SCR reaction through the nitrite route was faster than that through the nitrate route. Meanwhile, a new band at 1620 cm^{-1} appeared, which may be assigned adsorbed H_2O resulting from the SCR reaction. At last, $(Fe_{2.5}Mn_{0.5})_{1-\delta}O_4$ was mainly covered by adsorbed ammonia species (1450 and 1213 cm^{-1}). These results both suggest that some adsorbed nitrogen oxides took part in the SCR reaction.

At last, the IR spectra during the SCR reaction (i.e. NH_3 and NO + O_2 were simultaneously introduced) at 120 °C were recorded. As shown in Fig. 6a, the bands at 1444 cm^{-1} corresponding to adsorbed ammonia species appeared. The bands at 1546 and 1606 cm^{-1} corresponding to adsorbed monodentate nitrite cannot be observed. However, some slight adsorption at 1580 and 1520 cm^{-1} corresponding to bidentate nitrate can be detected. Bidentate nitrate resulted from the further oxidization of monodentate nitrite, so monodentate nitrite once formed. The intensity of adsorbed bidentate nitrate in Fig. 6a was much less than that in Fig. 5a. It indicates that the further oxidization of monodentate nitrite to bidentate nitrate was obviously restrained due to the presence of ammonia. Therefore, most of formed nitrite was eliminated by adsorbed ammonia species, and only a small amount of formed nitrite was further oxidized to bidentate nitrate. As a result, the contribution of bidentate nitrate to NO conversion might be neglected. As the reaction temperature increased from 120 to 180 °C, the adsorption species mainly corresponded to adsorbed ammonia species and its oxidization/deformation species, and the species corresponding to the adsorption of NO + O_2 can hardly be detected. It indicates that the adsorption of NO + O_2 on $(Fe_{2.5}Mn_{0.5})_{1-\delta}O_4$ may not happen in the presence of NH_3, or the formed monodentate nitrite and monodentate nitrate were quickly eliminated by adsorbed NH_3.

3.4. Mechanism and kinetic study

3.4.1. Mechanism

In situ DRIFTS study suggests that both the Eley–Rideal mechanism (i.e. reaction of activated ammonia with gaseous NO) and the Langmuir–Hinshelwood mechanism (i.e. reaction of adsorbed ammonia species with adsorbed NO_x species) [21] may happen during the SCR reaction over $(Fe_{3-x}Mn_x)_{1-\delta}O_4$.

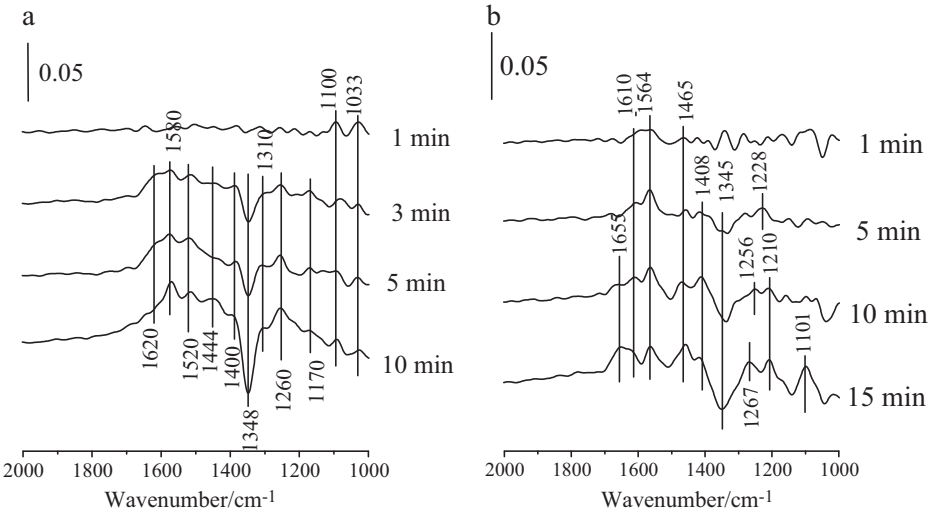

Fig. 6. DRIFT spectra taken upon passing $NH_3 + NO + O_2$ over $(Fe_{2.5}Mn_{0.5})_{1-\delta}O_4$: (a) 120 °C; (b) 180 °C.

The SCR reaction through the Langmuir–Hinshelwood mechanism can be approximately described as [21,41]:

$$NH_{3(g)} \rightleftharpoons NH_{3(ad)} \quad (2)$$

$$NO_{(g)} \rightleftharpoons NO_{(ad)} \quad (3)$$

$$\equiv Mn^{4+} - O + NO_{(ad)} \rightarrow \equiv Mn^{3+} + NO_2^- \quad (4)$$

$$\equiv Fe^{3+} - O + NO_{(ad)} \rightarrow \equiv Fe^{2+} + NO_2^- \quad (5)$$

$$NO_2^- + NH_3 \rightarrow \equiv N_2 + H_2O + OH^- \quad (6)$$

$$\equiv Mn^{3+} + \tfrac{1}{4}O_2 \rightarrow \equiv Mn^{4+} + \tfrac{1}{2} \equiv O \quad (7)$$

$$\equiv Fe^{2+} + \tfrac{1}{4}O_2 \rightarrow \equiv Fe^{3+} + \tfrac{1}{2} \equiv O \quad (8)$$

Reaction (2) was the adsorption of gaseous ammonia on the acid sites (i.e. Brønsted acid sites and Lewis acid sites) to form adsorbed ammonia species including ionic NH_4^+ and coordinated NH_3. There is general agreement that the SCR reaction starts with the adsorption of NH_3, which is very strong compared to the adsorption of $NO + O_2$ and the reaction products [21]. Reaction (3) was the adsorption of gaseous NO. Then the adsorbed NO was oxidized by Mn^{4+} and/or Fe^{3+} cations on the surface to form adsorbed NO_2^- (reactions (4) and (5)). The adsorption of $NO + O_2$ on γ-Fe_2O_3 was much weaker than those on $(Fe_{2.8}Mn_{0.2})_{1-\delta}O_4$ and $(Fe_{2.5}Mn_{0.2})_{1-\delta}O_4$ (shown in Fig. 4B). It indicates that the ability of Fe^{3+} cations to oxidize NO to NO_2^- was much less than that of Mn^{4+}. Therefore, Reaction (5) might be neglected if there were some Mn^{4+} cations on the surface. At last, the formed NO_2^- was reduced by adsorbed ammonia species to form N_2 and H_2O (reaction (6)). Reactions (7) and (8) were the re-oxidization of formed Mn^{3+} and Fe^{2+}.

The SCR reaction through the Eley–Rideal mechanism can be described as [41]:

$$NH_{3(g)} \rightleftharpoons NH_{3(d)} \quad (2)$$

$$NH_3 + \equiv Mn^{4+} \rightarrow -NH_2 + \equiv Mn^{3+} + H^+ \quad (9)$$

$$NH_3 + \equiv Fe^{3+} \rightarrow -NH_2 + \equiv Fe^{2+} + H^+ \quad (10)$$

$$-NH_2 + NO_{(g)} \rightarrow N_2 + H_2O \quad (11)$$

$$\equiv Mn^{3+} + \tfrac{1}{4}O_2 \rightarrow \equiv Mn^{4+} + \tfrac{1}{2} \equiv O \quad (7)$$

$$\equiv Fe^{2+} + \tfrac{1}{4}O_2 \rightarrow \equiv Fe^{3+} + \tfrac{1}{2} \equiv O \quad (8)$$

Reactions (9) and (10) were the activation of adsorbed ammonia species to form amide species ($-NH_2$) by Mn^{4+} and Fe^{3+} on the surface, respectively. Then, gaseous NO was reduced by $-NH_2$ on the surface to form N_2 and H_2O (reaction (11)).

3.4.2. Kinetic study

The concentration of NH_3 in the gas phase was sufficiently high for the surface to be saturated with adsorbed NH_3, so the concentration of NH_3 adsorbed on the surface ($[NH_{3(ad)}]$) at a specific temperature was an invariable and can be described as:

$$[NH_{3(ad)}] = k_1 c_{acid} \quad (12)$$

where k_1 and c_{acid} were a constant and the acidity on $(Fe_{3-x}Mn_x)_{1-\delta}O_4$, respectively. Reaction (2) was an exothermic reaction, so k_1 would rapidly decrease with the increase of reaction temperature (shown in Fig. 4A).

Meanwhile, the concentration of NO in the gas phase was also sufficiently high for the surface to be saturated with adsorbed NO, so the concentration of NO adsorbed on the surface ($[NO_{(ad)}]$) can be regarded as an invariable at a specific temperature. Reaction (3) was an exothermic reaction, so $[NO_{(ad)}]$ would rapidly decrease with the increase of reaction temperature.

The kinetic equation of reaction (4) can be described as:

$$-\frac{d[NO_{(ad)}]}{dt} = -\frac{d[Mn^{4+}]}{dt} = \frac{d[NO_2^-]}{dt} = k_2'[NO_{(ad)}][Mn^{4+}] \quad (13)$$

where k_2' was the kinetic constant of reaction (4). k_2' would increase with the increase of reaction temperature. Although k_2' increased with the increase of reaction temperature, $[NO_{(ad)}]$ decreased obviously. As a result, the adsorption of $NO + O_2$ obviously decreased as the reaction temperature increased from 120 to 180 °C (shown in Fig. 4 B).

During the SCR reaction, the reduction of NO adsorbed and Mn^{4+} on the surface can quickly recover through reactions (3) and (7), respectively. Therefore, both $[NO_{(ad)}]$ and $[Mn^{4+}]$ can be regarded as invariables. If the surface was saturated with the chemical adsorption of NO_2^-, the reduced NO_2^- through reaction (6) would quickly recover through reaction (4). As a result, the instantaneous concentration of NO_2^- on the surface ($[NO_2^-]$) may be regarded as an invariable at the steady state, and it was approximately propor-

tional to the product of $[NO_{(ad)}]$ and $[Mn^{4+}]$. Therefore, $[NO_2^-]$ can be described as:

$$[NO_2^-] = k_2[NO_{(ad)}][Mn^{4+}] \quad (14)$$

The kinetic equation of reaction (6) can be described as:

$$-\frac{d[NO_2^-]}{dt} = -\frac{d[NH_3]}{dt} = \frac{d[N_2]}{dt} = k_3[NO_2^-][NH_3]$$
$$= k_1k_2k_3[NO_{(ad)}][Mn^{4+}]c_{acid} \quad (15)$$

where k_3 was the kinetic constant of reaction (6). k_3 would increase with the increase of reaction temperature.

Therefore, the conversion of NO through the Langmuir–Hinshelwood mechanism can be described as:

$$-\frac{d[NO_{(g)}]}{dt}_{L-H} = k_1k_2k_3BET[NO_{(ad)}][Mn^{4+}]c_{acid}t' \quad (16)$$

where t' was the time how long the gas passed through the catalyst column. t' was equal to the reciprocal of GHSV.

The kinetic equation of reaction (9) can be described as:

$$-\frac{d[NH_{3(ad)}]}{dt} = -\frac{d[Mn^{4+}]}{dt} = \frac{d[NH_2]}{dt} = k'_4[NH_{3(ad)}][Mn^{4+}] \quad (17)$$

Meanwhile, the kinetic equation of reaction (10) can be described as:

$$-\frac{d[NH_{3(ad)}]}{dt} = -\frac{d[Fe^{3+}]}{dt} = \frac{d[NH_2]}{dt} = k'_5[NH_{3(ad)}][Fe^{3+}] \quad (18)$$

where k'_4 and k'_5 were the kinetic constants of reactions (9) and (10), respectively. They would increase with the increase of reaction temperature. As is well known, the oxidization ability of Mn^{4+} cations is much more than that of Fe^{3+} cations. Therefore, k_4 is much more than that of k_5. γ-Fe_2O_3 showed a moderate SCR activity above 140 °C (shown in Fig. 3a), so reaction (10) cannot be neglected.

During the SCR reaction, the reduced Mn^{4+}, Fe^{3+} and adsorbed NH_3 can recover through reactions (7), (8) and (2), respectively. Therefore, the concentrations of Mn^{4+} cation, Fe^{3+} cation and adsorbed NH_3 on $(Fe_{3-x}Mn_x)_{1-\delta}O_4$ ($[Mn^{4+}]$, $[Fe^{3+}]$ and $[NH_{3(ad)}]$) can be approximately regarded as invariables. If the surface was saturated with the chemical adsorption of $-NH_2$, the reduced $-NH_2$ through reaction (11) would quickly recover through reactions (7) and (8). As a result, the concentration of $-NH_2$ ($[-NH_2]$) at a steady state can be described as:

$$[NH_2] = k_4[NH_3][Mn^{4+}] + k_5[NH_3][Fe^{3+}] = k_1c_{acid}(k_4[\equiv Mn^{4+}]$$
$$+ k_5[Fe^{3+}]) = k_1k_6c_{acid} \quad (19)$$

$$k_6 = k_4[\equiv Mn^{4+}] + k_5[\equiv Fe^{3+}] \quad (20)$$

k_6 would increase with the increase of reaction temperature.

The kinetic equation of reaction (11) can be described as:

$$-\frac{d[-NH_2]}{dt} = -\frac{d[NO_{(g)}]}{dt} = \frac{d[N_2]}{dt} = k_7[-NH_2][NO_{(g)}] \quad (21)$$

where k_7 was the kinetic constant of reaction (11). k_7 would increase with the increase of reaction temperature.

Taking account of the reduction of gaseous NO through the Langmuir–Hinshelwood mechanism, the reduction of gaseous NO can be described as:

$$-\frac{d[NO_{(g)}]}{dt} = k_7[-NH_2][NO_{(g)}] + k_1k_2k_3[NO_{(ad)}][Mn^{4+}]c_{acid} \quad (22)$$

With the reduction of NO, the concentration of gaseous NO at the next section of catalyst column would gradually decrease. Because the GHSV was very high and the concentration of gaseous NO was generally much high than $[NO_{(ad)}]$, the concentration of gaseous NO at the specific section of catalyst column can be approximately described as:

$$[NO_{(g)}]_l = [NO_{(g)}]_0 \ \exp(-k_7[-NH_2]l) = [NO_{(g)}]_0$$
$$\times \ \exp(-k_1k_6k_7c_{acid}l) \quad (23)$$

where l was the time how long gaseous NO reached the specific section of catalyst column.

Therefore, the formed N_2 over the specific section of catalyst column can be described as:

$$\frac{d[N_2]_l}{dt} = k_1k_6k_7c_{acid}[NO_{(g)}]_0 \ \exp(-k_1k_6k_7c_{acid}l) \quad (24)$$

The amount of N_2 formed over the whole catalyst column can then be described as:

$$\frac{d[N_2]}{dt} = k_1k_6k_7c_{acid}[NO_{(g)}]_0\int_0^{t'}\exp(-k_1k_6k_7c_{acid}l)dl \quad (25)$$

Therefore, the conversion of NO through the Eley–Rideal mechanism can be approximately described as:

$$-\frac{d[NO_{(g)}]}{dt}_{E-R} = BETk_1k_6k_7c_{acid}[NO_{(g)}]_0\int_0^{t'}\exp(-k_1k_6k_7c_{acid}l)dl \quad (26)$$

The total conversion of NO through both the Eley–Rideal mechanism and the Langmuir–Hinshelwood mechanism can be described as:

$$-\frac{d[NO_{(g)}]}{dt} = k_1k_6k_7BETc_{acid}[NO_{(g)}]_0\int_0^{t'}\exp(-k_1k_6k_7c_{acid}l)dl$$
$$+ BETk_1k_2k_3[NO_{(ad)}][Mn^{4+}]c_{acid}t' \quad (27)$$

Then, the ratio of NO conversion can be described as:

$$X = k_1k_6k_7BETc_{acid}\int_0^{t'}\exp(-k_1k_6k_7c_{acid}l)dl + k_1k_2k_3BET[Mn^{4+}]$$
$$\times c_{acid}t'\frac{[NO_{(ad)}]}{[NO_{(g)}]_0} \quad (28)$$

As shown in Tables 1 and 2, the BET surface area, the acidity and the concentration of Mn^{4+} of/on $(Fe_{2.5}Mn_{0.5})_{1-\delta}O_4$ was more than those of/on $(Fe_{2.8}Mn_{0.2})_{1-\delta}O_4$. Therefore, the SCR activity of $(Fe_{2.5}Mn_{0.5})_{1-\delta}O_4$ was much better than that of $(Fe_{2.8}Mn_{0.2})_{1-\delta}O_4$.

To determine the order of SCR reaction with respect to NH_3, the concentration of NO was kept constantly at 500 ppm, while the concentration of NH_3 varied from 500 to 1500 ppm. To determine the order with respect to NO, the concentration of NO varied from 500 to 1500 ppm, in which the concentration of NH_3 was equal to that of NO to keep it enough for the SCR reaction. As shown in Fig. 7a, the ratio of NO conversion on $(Fe_{2.5}Mn_{0.5})_{1-\delta}O_4$ did not obviously change as the ratio of NH_3 to NO varied from 1 to 3. This was hinted by Eq. (28). It was also consistent with previous researches [23,42]. If the SCR reaction over $(Fe_{2.5}Mn_{0.5})_{1-\delta}O_4$ mainly followed the Eley–Rideal mechanism, the ratio of NO conversion should not decrease with the increase of NO concentration from 500 ppm to 1500 ppm. If the SCR reaction over $(Fe_{2.5}Mn_{0.5})_{1-\delta}O_4$ mainly followed the Langmuir–Hinshelwood mechanism, the ratio of NO conversion should halve after NO concentration or GHSV was doubled. After doubling NO concentration or GHSV, the ratio of NO conversion obviously decreased especially below 160 °C (shown in Fig. 7b and c). However, the ratio of NO conversion did not halve. These results demonstrate that both the Eley–Rideal mechanism

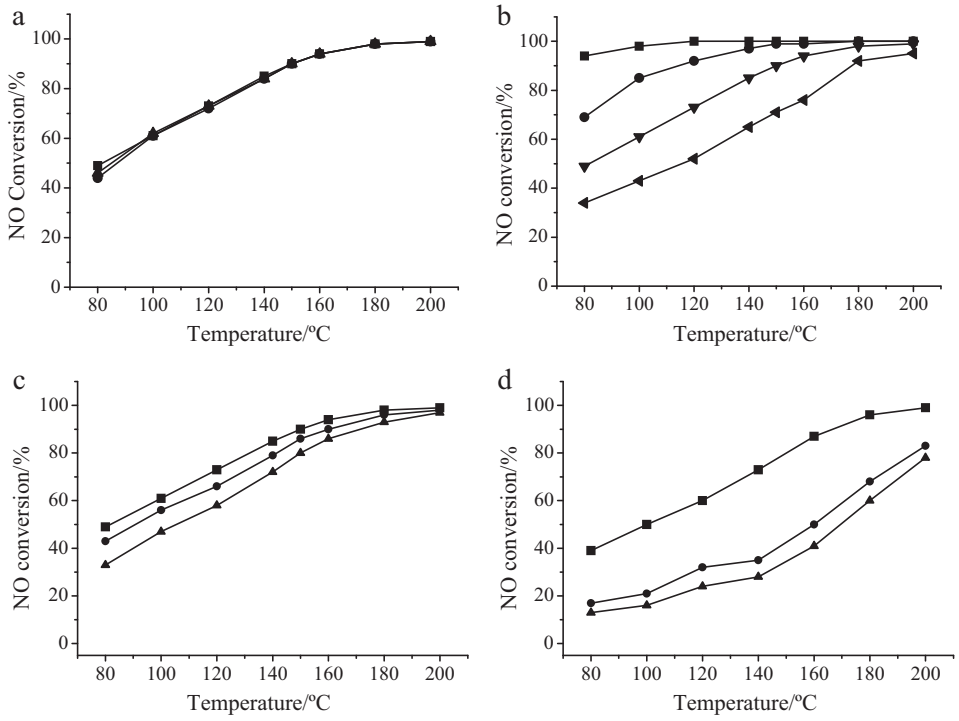

Fig. 7. (a) Influence of the concentration of NH_3 on NO conversion over $(Fe_{2.5}Mn_{0.5})_{1-\delta}O_4$, [NO] = 500 ppm, $[O_2]$ = 2 vol%, catalyst mass = 100 mg, total flow rate = 200 mL min^{-1}: ■, $[NH_3]$ = 500 ppm; •, 1000 ppm; ▲, 1500 ppm. (b) Influence of GHSV on NO conversion over $(Fe_{2.5}Mn_{0.5})_{1-\delta}O_4$, [NO] = $[NH_3]$ = 500 ppm, $[O_2]$ = 2 vol%, GHSV = ■, 30,000 h^{-1}; ●, 75,000 h^{-1}; ▲, 150,000 h^{-1}; ◄, 300,000 h^{-1}. (c) Influence of the concentration of NO on NO conversion over $(Fe_{2.5}Mn_{0.5})_{1-\delta}O_4$: ■, [NO] = $[NH_3]$ = 500 ppm; •, [NO] = $[NH_3]$ = 1000 ppm; ▲, [NO] = $[NH_3]$ = 1500 ppm. $[O_2]$ = 2 vol%, catalyst mass = 100 mg, total flow rate = 200 mL min^{-1} and GHSV = 150,000 h^{-1}. (d) Influence of the concentration of NO on NO conversion over $(Fe_{2.8}Mn_{0.2})_{1-\delta}O_4$: ■, [NO] = $[NH_3]$ = 500 ppm; •, [NO] = $[NH_3]$ = 1000 ppm; ▲, [NO] = $[NH_3]$ = 1500 ppm. $[O_2]$ = 2 vol%, catalyst mass = 100 mg, total flow rate = 200 mL min^{-1} and GHSV = 150,000 h^{-1}.

and the Langmuir–Hinshelwood mechanism contributed to the SCR reaction.

According to Eq. (28), the specific contribution of the two mechanism to the SCR reaction over $(Fe_{3-x}Mn_x)_{1-\delta}O_4$ at the specific reaction condition ([NO] = $[NH_3]$ = 500 ppm, $[O_2]$ = 2 vol% and GHSV = 150,000 h^{-1}) can be calculated after adjusting gaseous NO concentration (shown in Fig. 7c and d). As shown in Fig. 8a, most of the conversion of NO over $(Fe_{2.8}Mn_{0.2})_{1-\delta}O_4$ followed the Langmuir–Hinshelwood mechanism below 180 °C, especially at lower temperatures. Meanwhile, the SCR reaction through the Eley–Rideal mechanism obviously promoted with the increase of reaction temperature. However, most of the conversion of NO over $(Fe_{2.5}Mn_{0.5})_{1-\delta}O_4$ followed the Eley–Rideal mechanism, and its contribution to NO conversion increased with the increase of reaction temperature (shown in Fig. 8b).

As 6.7% of Fe^{3+} cations were substituted by Mn cations, the adsorption of NO + O_2 on $(Fe_{2.8}Mn_{0.2})_{1-\delta}O_4$ at 120 °C was obviously promoted (shown in Fig. 4B). However, the adsorption of NH_3 was not promoted (shown in Fig. 4A). Therefore, the concentration of adsorbed NO was much higher than that of adsorbed NH_3 on $(Fe_{2.8}Mn_{0.2})_{1-\delta}O_4$. Then, Mn^{4+} and Fe^{3+} cations on the surface may prefer to oxidize adsorbed NO (reactions (4) and (5)) rather than adsorbed NH_3 (reactions (9) and (10)). As a result, the Langmuir–Hinshelwood mechanism predominated over the SCR reaction over $(Fe_{2.8}Mn_{0.2})_{1-\delta}O_4$ below 180 °C. Although k_2 and k_3 increased with the increase of reaction temperature, k_1 and $[NO_{(ad)}]$ decreased (shown in Eq. (15)). As a result, NO conversion over $(Fe_{2.8}Mn_{0.2})_{1-\delta}O_4$ through the Langmuir–Hinshelwood mechanism increased with the increase of reaction temperature from 80 to 160 °C. With the further increase of reaction temperature, it decreased. Although k_1 decreased with the increase of reaction temperature, k_6 and k_7 obviously increased. As a result, NO conversion over $(Fe_{2.8}Mn_{0.2})_{1-\delta}O_4$

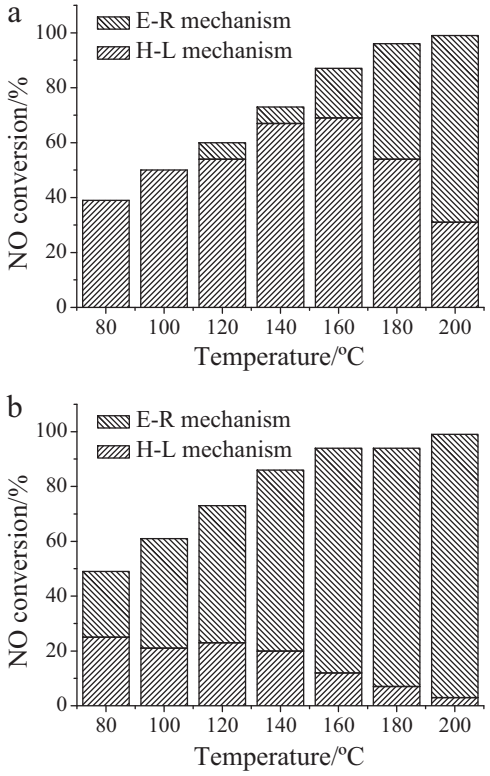

Fig. 8. Contribution of the Eley–Rideal mechanism and the Langmuir–Hinshelwood mechanism to the SCR reaction over $(Fe_{3-x}Mn_x)_{1-\delta}O_4$. (a) x = 0.2; (b) x = 0.5. Reaction condition: [NO] = $[NH_3]$ = 500 ppm, $[O_2]$ = 2 vol%, N_2 balance, catalyst mass = 100 mg, total flow rate = 200 mL min^{-1} and GHSV = 150,000 h^{-1}.

through the Eley–Rideal mechanism gradually increased with the increase of reaction temperature.

With the further incorporation of Mn into γ-Fe_2O_3, both the adsorption of NO + O_2 and the adsorption NH_3 on $(Fe_{2.5}Mn_{0.5})_{1-\delta}O_4$ were obviously promoted (shown in Fig. 4). Furthermore, the decrease of adsorbed NO + O_2 was much faster than that of adsorbed ammonia (shown in Fig. 4). Therefore, the concentration of adsorbed NH_3 may be much higher than that of adsorbed NO on $(Fe_{2.5}Mn_{0.5})_{1-\delta}O_4$, especially at higher temperatures. Then, Mn^{4+} and Fe^{3+} cations on $(Fe_{2.5}Mn_{0.5})_{1-\delta}O_4$ may prefer to oxidize adsorbed NH_3 rather than adsorbed NO. As a result, the Eley–Rideal mechanism predominated over the SCR reaction over $(Fe_{2.5}Mn_{0.5})_{1-\delta}O_4$, especially at higher temperatures (shown in Fig. 8b).

3.5. Origination of N_2O

Fig. 3b shows that some N_2O formed during the SCR reaction over $(Fe_{3-x}Mn_x)_{1-\delta}O_4$ and the amount of N_2O formed increased with the increase of reaction temperature and Mn content.

Both the Langmuir–Hinshelwood mechanism (i.e. the nitrate route, reaction (29)) and the Eley–Rideal mechanism (i.e. the over-oxidization of adsorbed ammonia species, reactions (30) and (31)) can generate N_2O [21,41,43]. The kinetic process of the nitrate route was similar that of nitrite route (reactions (2)–(8)), and the kinetic process of the over-oxidization of adsorbed ammonia species was similar that of amide route (reactions (2) and (7)–(11)). Therefore, the contribution of the Langmuir–Hinshelwood mechanism and the Eley–Rideal mechanism to the SCR reaction may not change even if reactions (29)–(31) happened.

$$NH_3 + NO_3^- \rightarrow N_2O + H_2O + OH^- \quad (29)$$

$$NH_3 + \equiv Mn^{4+} \rightarrow -NH + \equiv Mn^{2+} + 2H^+ \quad (30)$$

$$-NH + NO_{(g)} \rightarrow N_2O + H^+ \quad (31)$$

Fig. 8a indicates that both the Langmuir–Hinshelwood mechanism and the Eley–Rideal mechanism happened during the SCR reaction over $(Fe_{2.8}Mn_{0.2})_{1-\delta}O_4$ above 140 °C. Therefore, N_2O formed over $(Fe_{2.8}Mn_{0.2})_{1-\delta}O_4$ resulted from both the nitrate route and the over-oxidization of adsorbed ammonia. Fig. 8b suggests that the Eley–Rideal mechanism predominated over the SCR reaction over $(Fe_{2.5}Mn_{0.5})_{1-\delta}O_4$ above 160 °C. Therefore, N_2O formed over $(Fe_{2.5}Mn_{0.5})_{1-\delta}O_4$ may mainly result from the over-oxidization of adsorbed ammonia.

3.6. Effect of H_2O and SO_2

There is still residual SO_2 remaining after the desulfurizer, which obviously interferes with the low temperature SCR reaction [23,44]. Furthermore, water vapor is one of the main components in the flue gas and often leads to the deactivation of catalysts. Therefore, the synergetic effect of H_2O and SO_2 on the SCR activity of $(Fe_{2.5}Mn_{0.5})_{1-\delta}O_4$ was investigated. After the addition of H_2O and SO_2 for 100 min, the ratio of NO conversion decreased from 100% to about 60% (shown in Fig. 9). It indicates that the SCR activity of $(Fe_{2.5}Mn_{0.5})_{1-\delta}O_4$ was intensively suppressed in the presence of H_2O and SO_2. This result was consistent with the researches on other Mn based catalysts [19,44,45]. The deactivation of low temperature SCR catalysts may mainly be attributed to the deposition of ammonium bisulfate [23,45]. Fig. 9 shows that the ratio of NO conversion can recover to 100% after the deactivated catalyst was washed by water. It indicates that the deactivated catalyst can be regenerated after the water washing due to the water solubility of ammonium bisulfate. Therefore, the effect of H_2O and SO_2 on the SCR reaction over $(Fe_{2.5}Mn_{0.5})_{1-\delta}O_4$ could be minimized after periodic operation of water washing.

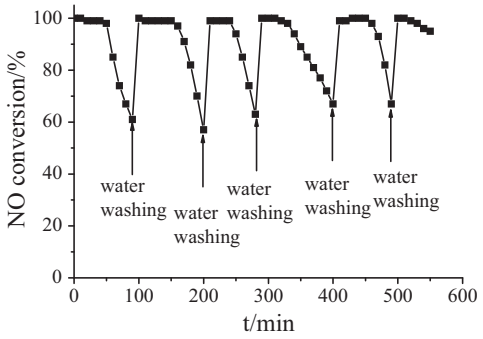

Fig. 9. Effect of H_2O and SO_2 on the SCR activity of $(Fe_{2.5}Mn_{0.5})_{1-\delta}O_4$, reaction condition: [NO] = 500 ppm, [NH_3] = 550 ppm, [O_2] = 2 vol%, [SO_2] = 50 ppm, [H_2O] = 5%, N_2 balance and GHSV = 15,000 h^{-1}.

4. Conclusion

Mn–Fe spinel, a low temperature SCR catalyst, was synthesized using a co-precipitation method. The adsorption of NO + O_2 or/and the adsorption of NH_3 on $(Fe_{3-x}Mn_x)_{1-\delta}O_4$ were obviously promoted due to the incorporation of Mn into γ-Fe_2O_3. As a result, the SCR activity of $(Fe_{3-x}Mn_x)_{1-\delta}O_4$ increased with the increase of Mn content. $(Fe_{2.5}Mn_{0.5})_{1-\delta}O_4$ showed excellent activity and selectivity at 80–160 °C. The SCR reaction over $(Fe_{2.5}Mn_{0.5})_{1-\delta}O_4$ mainly followed the Eley–Rideal mechanism. N_2O formed on $(Fe_{2.5}Mn_{0.5})_{1-\delta}O_4$ above 160 °C mainly resulted from the over-oxidization of adsorbed ammonia species. $(Fe_{2.5}Mn_{0.5})_{1-\delta}O_4$ deactivated by H_2O and SO_2 can be regenerated after the water washing.

Acknowledgments

This study was financially supported by the National Natural Science Fund of China (grant no. 51078203), the National High-Tech Research and Development (863) Program of China (grant nos. 2010AA065002 and 2009AA06Z301) and the Scholarship Award for Excellent Doctoral Student granted by Ministry of Education of China.

References

[1] J.H. Li, W.H. Goh, X.C. Yang, R.T. Yang, Appl. Catal. B: Environ. 90 (2009) 360–367.
[2] G.H. Jing, J.H. Li, D. Yang, J.M. Hao, Appl. Catal. B: Environ. 91 (2009) 123–134.
[3] F.D. Liu, K. Asakura, H. He, W.P. Shan, X.Y. Shi, C.B. Zhang, Appl. Catal. B: Environ. 103 (2010) 369–377.
[4] L. Chen, J.H. Li, M.F. Ge, Environ. Sci. Technol. 44 (2010) 9590–9596.
[5] J.H. Li, R.H. Zhu, Y.S. Cheng, C.K. Lambert, R.T. Yang, Environ. Sci. Technol. 44 1799–1805.
[6] L. Chen, J.H. Li, M.F. Ge, J. Phys. Chem. C 113 (2009) 21177–21184.
[7] L. Chen, J.H. Li, M.F. Ge, R.H. Zhu, Catal. Today 153 77–83.
[8] F. Liu, H. He, C. Zhang, Chem. Commun. 17 (2008) 2043–2045.
[9] F.D. Liu, H. He, J. Phys. Chem. C 114 (2010) 16929–16936.
[10] F.D. Liu, H. He, Y. Ding, C.B. Zhang, Appl. Catal. B: Environ. 93 (2009) 194–204.
[11] L. Ma, J.H. Li, R. Ke, L.X. Fu, J. Phys. Chem. C 115 (2011) 7603–7612.
[12] N. Apostolescu, B. Geiger, K. Hizbullah, M.T. Jan, S. Kureti, D. Reichert, F. Schott, W. Weisweiler, Appl. Catal. B: Environ. 62 (2006) 104–114.
[13] X. Gao, X.S. Du, L.W. Cui, Y.C. Fu, Z.Y. Luo, K.F. Cen, Catal. Commun. 12 255–258.
[14] T. Valdes-Solis, G. Marban, A.B. Fuertes, Appl. Catal. B: Environ. 46 (2003) 261–271.
[15] D.K. Sun, Q.Y. Liu, Z.Y. Liu, G.Q. Gui, Z.G. Huang, Appl. Catal. B: Environ. 92 (2009) 462–467.
[16] H.H. Phil, M.P. Reddy, P.A. Kumar, L.K. Ju, J.S. Hyo, Appl. Catal. B: Environ. 78 (2008) 301–308.
[17] P. Lu, C.T. Li, G.M. Zeng, L.J. He, D.L. Peng, H.F. Cui, S.H. Li, Y.B. Zhai, Appl. Catal. B: Environ. 96 (2010) 157–161.
[18] M. Casapu, O. Krocher, M. Elsener, Appl. Catal. B: Environ. 88 (2009) 413–419.
[19] Z.H. Chen, Q. Yang, H. Li, X.H. Li, L.F. Wang, S.C. Tsang, J. Catal. 276 (2011) 56–65.

[20] F. Eigenmann, M. Maciejewski, A. Baiker, Appl. Catal. B: Environ. 62 (2006) 311–318.
[21] W.S. Kijlstra, D.S. Brands, H.I. Smit, E.K. Poels, A. Bliek, J. Catal. 171 (1997) 219–230.
[22] G.S. Qi, R.T. Yang, Appl. Catal. B: Environ. 44 (2003) 217–225.
[23] G.S. Qi, R.T. Yang, J. Catal. 217 (2003) 434–441.
[24] G.S. Qi, R.T. Yang, Chem. Commun. 7 (2003) 848–849.
[25] G.S. Qi, R.T. Yang, J. Phys. Chem. B 108 (2004) 15738–15747.
[26] G.S. Qi, R.T. Yang, R. Chang, Appl. Catal. B: Environ. 51 (2004) 93–106.
[27] J. Yu, F. Guo, Y.L. Wang, J.H. Zhu, Y.Y. Liu, F.B. Su, S.Q. Gao, G.W. Xu, Appl. Catal. B: Environ. 95 (2010) 160–168.
[28] P.R. Ettireddy, N. Ettireddy, S. Mamedov, P. Boolchand, P.G. Smirniotis, Appl. Catal. B: Environ. 76 (2007) 123–134.
[29] Z. Wu, B.Q. Jiang, Y. Liu, Appl. Catal. B: Environ. 79 (2008) 347–355.
[30] Z.J. Zhang, Z.L. Wang, B.C. Chakoumakos, J.S. Yin, J. Am. Chem. Soc. 120 (1998) 1800–1804.
[31] S. Yang, N. Yan, Y. Guo, D. Wu, H. He, Z. Qu, J. Li, Q. Zhou, J. Jia, Environ. Sci. Technol. 45 (2011) 1540–1546.
[32] T. Kodama, M. Ookubo, S. Miura, Y. Kitayama, Mater. Res. Bull. 31 (1996) 1501–1512.
[33] B. Gillot, M. Laarj, S. Kacim, J. Mater. Chem. 7 (1997) 827–831.
[34] Y.J. Kim, H.J. Kwon, I.S. Nam, J.W. Choung, J.K. Kil, H.J. Kim, M.S. Cha, G.K. Yeo, Catal. Today 151 244–250.
[35] S. Yang, Y. Guo, N. Yan, D. Wu, H. He, Z. Qu, C. Yang, Q. Zhou, J. Jia, ACS Appl. Mater. Interfaces 3 (2011) 209–217.
[36] S. Yang, Y. Guo, N. Yan, D. Wu, H. He, J. Xie, Z. Qu, J. Jia, Appl. Catal. B: Environ. 101 (2011) 698–708.
[37] S. Yang, Y. Guo, N. Yan, Z. Qu, J. Xie, C. Yang, J. Jia, J. Hazard. Mater. 186 (2011) 508–515.
[38] L. Singoredjo, R. Korver, F. Kapteijn, J. Moulijn, Appl. Catal. B: Environ. 1 (1992) 297–316.
[39] F. Kapteijn, L. Singoredjo, N.J.J. Dekker, J.A. Moulijn, Ind. Eng. Chem. Res. 32 (1993) 445–452.
[40] K.I. Hadjiivanov, Catal. Rev. 42 (2000) 71–144.
[41] G. Busca, L. Lietti, G. Ramis, F. Berti, Appl. Catal. B: Environ. 18 (1998) 1–36.
[42] R.Q. Long, R.T. Yang, J. Catal. 190 (2000) 22–31.
[43] X.F. Tang, J.H. Li, L.A. Sun, J.M. Hao, Appl. Catal. B: Environ. 99 (2010) 156–162.
[44] W.S. Kijlstra, M. Biervliet, E.K. Poels, A. Bliek, Appl. Catal. B: Environ. 16 (1998) 327–337.
[45] R.Q. Long, R.T. Yang, R. Chang, Chem. Commun. 5 (2002) 452–453.